ACS APPLIED MATERIALS & INTERFACES

Research Article

www.acsami.org

Effective Piezoelectric Response of Substrate-Integrated ZnO Nanowire Array Devices on Galvanized Steel

By Jesus M. Velazquez,[†] Sivapalan Baskaran,[‡] Anil V. Gaikwad,[§] Tam-Triet Ngo-Duc,[⊥] Xiangtong He,[‡] Michael M. Oye,[⊥] M. Meyyappan,[⊥] Tapan K. Rout,[§] John Y. Fu,[‡] and Sarbajit Banerjee*[,†]

[†]Department of Chemistry, University at Buffalo, The State University of New York, Buffalo, New York 14260-3000, United States

[‡]Department of Mechanical and Aerospace Engineering, University at Buffalo, The State University of New York, Buffalo, New York 14260, United States

[§]Research, Development and Technology, Tata Steel Group (Europe), 1760 Ijmuiden, The Netherlands

[⊥]Center for Nanotechnology, NASA Ames Research Center, Moffett Field, California 94035, United States

Supporting Information

ABSTRACT: Harvesting waste energy through electromechanical coupling in practical devices requires combining device design with the development of synthetic strategies for large-area controlled fabrication of active piezoelectric materials. Here, we show a facile route to the large-area fabrication of ZnO nanostructured arrays using commodity galvanized steel as the Zn precursor as well as the substrate. The ZnO nanowires are further integrated within a device construct and the effective piezoelectric response is deduced based on a novel experimental approach involving induction of stress in the nanowires through pressure wave propagation along with phase-selective lock-in detection of the induced current. The robust methodology for measurement of the effective piezoelectric coefficient developed here allows for interrogation of piezoelectric functionality for the entire substrate under bending-type deformation of the ZnO nanowires.

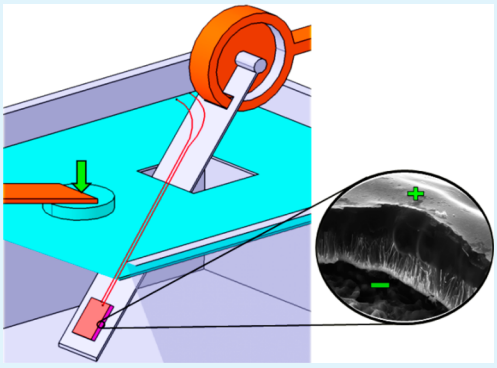

KEYWORDS: *electromechanical devices, functional coatings, galvanized steel, nanowire array, piezoelectric coefficient, zinc oxide*

There has been tremendous emphasis worldwide on developing photovoltaic, thermoelectric, and piezoelectric modes of power generation in an attempt to tackle the impending energy crisis. In this context, the remarkable alterations in the physical properties of periodic solids induced upon scaling to finite size have led to novel devices with transformative, often disruptive, potential for impact on a wide range of technological areas spanning energy generation and storage, electronics, and sensors.[1−6] However, realization of the promise of nanotechnology depends upon establishing industrial viability, which requires a restrictive combination of ease of manufacturing of the constituent nanomaterials, efficient routes towards device integration, and robustness of performance over prolonged periods of operation.

Much effort has been invested thus far on the integration of ZnO nanostructures within device constructs for energy harvesting, particularly for photovoltaic cells and piezoelectric nanogenerators.[5,7−9] The latter concept, championed by Wang, is attractive to scavenge mechanical energy from ubiquitous sources such as the human body, flowing water, and vehicular motion. Self-powered piezoelectric nanogenerators can be envisioned in applications wherein changing of batteries is an especially onerous task, such as remote sensing, implantable biomedical devices, and satellite applications. Although the piezoelectric constant of ZnO is smaller than that of perovskites such as the lead zirconium titanate (PZT) family,[10] much effective functionality can be derived from this simple binary oxide in nanoscale form because of the large mechanical deflections that can be sustained by ZnO nanostructures, their resistance to fatigue, and the potential to tune the Fermi surfaces at metal contacts to this semiconductor.[5]

The unique well-aligned substrate-integrated nanowire arrays and their facile production route represent major breakthroughs since they permit the fabrication of large-area piezoelectric power generators on commodity galvanized steel substrates that are available at low cost. Galvanization of steel has been practiced for nearly hundred years and remains the most reliable method for protecting low alloy steels from corrosion.[11] Electroactive zinc coatings serve both as barriers precluding transport of corroding species to the underlying metal substrate as well as providing sacrificial protection by virtue of the established differential in reduction potentials. Herein, we demonstrate that the galvanized Zn coating need not simply serve as a passive protective layer but can be endowed with further functionality through integration of a piezoelectric device. We further illustrate a novel phase-selective detection

Received: July 8, 2013
Accepted: October 1, 2013
Published: October 1, 2013

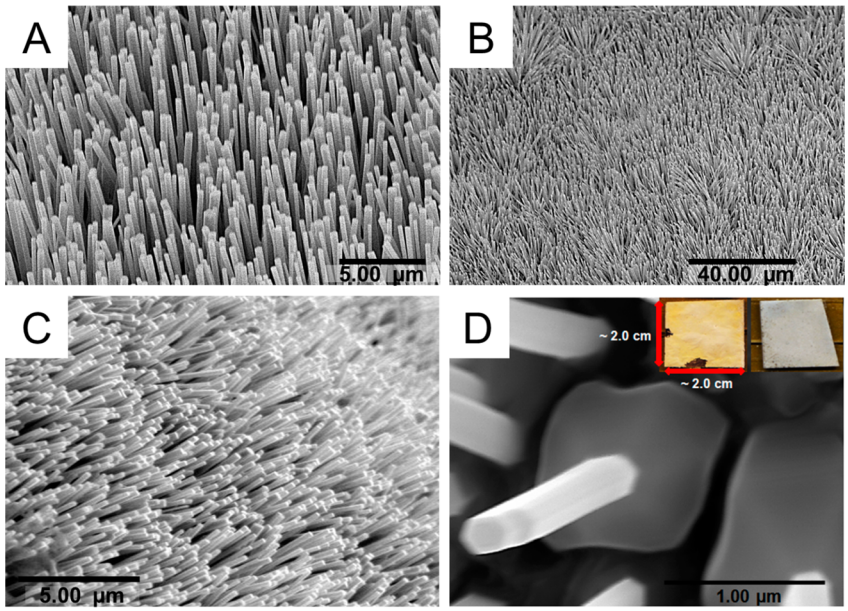

Figure 1. Scanning electron micrographs of ZnO arrays. (A) Highly oriented ZnO nanowires, (B, C) Large-area homogenous surface coverage of ZnO nanowires on steel. (D) Top view of a single ZnO nanowire, showing a characteristic hexagonal shape at the tip (inset-full coverage of ZnO nanowire arrays on galvanized steel substrates).

scheme that allows for measurement of the intrinsic piezoelectric response of ZnO nanowires (NWs).

Wang et al. have advanced a mechanism for piezoelectric power generation from nanoscale ZnO structures based on the deflection-induced creation of bound surface charges within the nanostructures.[5,7−9] The accumulated piezoelectric polarization can be transformed into charge flow through an appropriate read-out circuit when a Schottky barrier at one (or both) ZnO/metal interfaces is appropriately biased with respect to the piezoelectric potential. These authors have devised several elegant piezoelectric devices based on the same fundamental operating principles. Some examples of the device concepts include a scanning probe tip contacting and deflecting individual ZnO NWs, an ultrasonically actuated array of ZnO NWs contacted at the top with a zigzag electrode, piezoelectric fine wires with intermeshing Au and ZnO NW arrays, laterally aligned NW arrays laying atop a substrate that is subjected to flexion, and vertically integrated NWs packaged within polymer films, which yield enhanced current and voltage values.[5,7−9,12,13] We present here an inexpensive approach for the fabrication of large-area ZnO nanowires/nanostructures integrated onto earth-abundant commodity galvanized steel substrates and further illustrate a simple device design and measurement methodology that allows for reliable evaluation of the effective composite piezoelectric coefficient as a function of angular deformation of the nanowires, thereby directly showing the potential application of these systems.

In previous work, we have demonstrated that low alloy steel surfaces can catalyze the growth of carbon nanotube (CNT) arrays upon exposure to carbonaceous precursors and a reducing environment.[14] Upon appropriate oxidative processing these substrates further yield α-Fe_2O_3 nanowires.[15] Simple oxidative processing of galvanized steel analogously yields a variety of ZnO nanostructures as depicted in Figures 1 and Figure S1 in the Supporting Information. The piezoelectric effect in ZnO is derived from the polar nature of chemical bonding and the absence of a center of symmetry in its crystal structure.[5,7,8] The Zn^{2+} and O^{2-} ions are both tetrahedrally coordinated with the structural overlap allowing for charge neutralization under strain-free conditions, as depicted in Figure S2 in the Supporting Information. However, when subjected to a uniform mechanical stress, the apices of the cation- and anion-centered tetrahedra are slightly displaced, resulting in residual polarization.

RESULTS

Synthesis and Characterization of ZnO Nanostructures. Figure 1 depicts highly oriented ZnO nanowires conformally aligned across large areas obtained under O_2 flow on galvanized steel substrates without the use of any extraneous catalysts. The nanowires range in diameter from ∼100−200 nm and are several micrometers long. The inset to Figure 1D indicates the complete and homogenous coverage of macroscopic samples with ZnO nanowires; the coverage of the arrays is limited only by the dimensions of our vapor transport system. Under appropriate conditions (1000−1600 sccm of Ar and 2.5 sccm of O_2), the nanowires remain well-adhered to the underlying steel substrates (verified by ASTM D-3359), enabling the fabrication of robust substrate-integrated ZnO nanowire arrays suitable for use in structural applications. The well-adhered ZnO nanowires have been used for the piezoelectric experiments described below.

As seen previously for carbothermal growth of ZnO nanowires,[7,16] the morphologies and degree of alignment of ZnO NW arrays depend sensitively upon the partial pressures of the oxygen and zinc precursors. Figure 1D shows an individual ZnO nanowire growing from a fractured island of Zn; molten/vaporized Zn species serve as monomeric precursors after an initial nucleation event. The degree of supersaturation and monomer depletion is distinct on the two surfaces of galvanized steel and indeed "nanocomb"-like structures are obtained from the bottom surface (see Figure S1 in the Supporting Information). Growth in an open air ambient yields networks of ZnO tetrapods, as depicted in Figure S1B in the Supporting Information. Further reducing

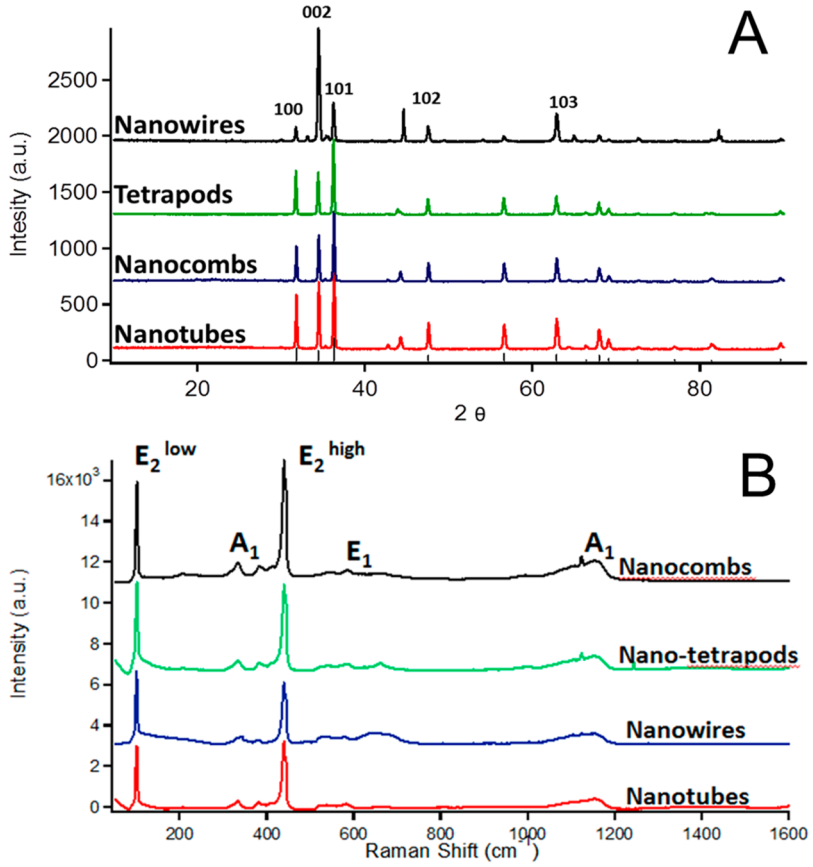

Figure 2. (A) Indexed X-ray diffraction patterns of ZnO nanostructures. (B) Raman spectra acquired for ZnO nanostructures at 514.5 nm laser excitation. The phonon mode assignments are labeled in the figure and correspond to characteristic zincite phonons.

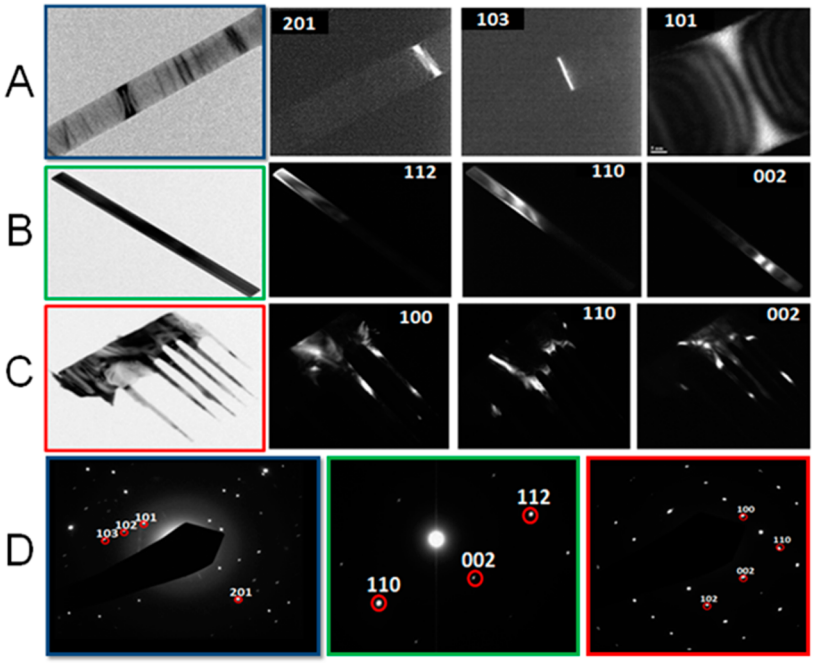

Figure 3. Bright- and dark-field transmission electron microscopy (TEM) images along with selected area electron difraction (SAED) patterns of ZnO nanostructures. (A) Left panel shows one arm of a nanotetrapod; the subsequent three panels show aperture-deflected dark-field TEM images. The images have been collected and indexed using the SAED pattern in (D, left). (B) Left panel shows the bright-field image of an individual nanowire, whereas the subsequent three panels indicate twist contours visible under dark-field TEM imaging. (C) Left panel shows the bright field image of a nanocomb, whereas subsequent panels indicate dark-field images acquired at different aperture displacements indicating twist contours within each of the individual pins. (D) SAED patterns acquired for nanotetrapods (blue), nanowires (green), and nanocombs (red).

the system pressure yields inhomogeneous islands of ZnO nanotubes (see Figure S3 in the Supporting Information). All these morphologies are obtained simply by altering the O_2 and Ar partial pressures (thereby also the Zn monomer concentration) without the addition of any catalysts, templates, or structure-directing agents.

Figure 2A shows X-ray diffraction (XRD) patterns acquired for the as-synthesized ZnO nanostructures. The reflections for all the samples can be indexed to characteristic peaks of hexagonal *syn*-ZnO, zincite (International Centre for Diffraction Data (ICDD) No. 01-080-0075). Preferential growth along the {001} direction is evidenced for the ZnO nanowire arrays, wherein the (002) reflection is the most pronounced. The phase identification has been further corroborated by the Raman spectra depicted in Figure 2B.[17]

The bright-field TEM images for ZnO nanostructures (Figure 3A−C) indicate clear modulation in contrast arising from contour profiles that result from twisting of the zincite crystal lattice. The corresponding selected-area electron diffraction (SAED) patterns are shown in Figure 3D. The SAED patterns have been used to acquire aperture-deflected dark-field images, wherein twist contours are discernible and can be systematically indexed.

Under conditions of low-to-moderate supersaturation, Morin et al. have emphasized that layer-by-layer crystal growth can be energetically prohibitive, and instead anisotropic growth occurs through the propagation of axial screw dislocations.[18,19] Growth along spiral screw dislocations with a linear dependence on the supersaturation is well established in classical Burton−Cabrera−Frank crystallization theory but has been underappreciated for nanomaterials until the work by Jin and coworkers.[19,20] Essentially, a screw dislocation generates substantial strain energy within the crystal, which is relieved either through formation of an inner surface and concomitant voiding of the interior or through establishment of a torque that twists the quasi-cylindrical nanowire (the Eshelby twist).[18,19] Unlike in Morin's work, a constant flow rate of Zn precursors is unlikely here given the rapid ramp rates and the fact that depletion of the monomer and eventual crystal growth occurs in the same region. Notwithstanding the more complex kinetics, some phenomenological parallels can be drawn based on TEM imaging of the nanostructures. The bright-field TEM images for ZnO nanostructures (Figure 3A−C) indicate clear modulation in contrast arising from contour profiles that result from twisting of the zincite crystal lattice. The corresponding selected-area electron diffraction (SAED) patterns are shown in Figure 3D. The SAED patterns have been used to acquire aperture-deflected dark-field images, wherein the twist contours are prominently discernible and can be systematically indexed. Indeed, the SEM images in Figure S3 in the Supporting Information illustrating growth of ZnO nanotubes further corroborate such a mechanism because strain energy from a screw dislocation can also quite efficiently be relieved through creation of an inner surface.

From the perspective of piezoelectric power generation, anisotropic growth along the crystallographic *c* axis is especially desirable (see Figure S2 in the Supporting Information) and indeed the screw-dislocation-driven mechanism yields nanowires with good crystallographic alignment, as indicated by the XRD pattern in Figure 2A. Although the twist contours reflect the presence of dislocations that may have a deleterious impact, such dislocations are expected to be unstable within small volumes, leading to ready elimination upon actuation.[18]

Piezoelectric Measurements of ZnO Nanowire Arrays. Although the piezoelectric coefficient of ZnO is fairly modest in the bulk, there is some evidence that enhanced polarization can be induced at nanoscale dimensions as a result of surface reconstruction.[21] The biocompatibility of ZnO further represents a significant advantage given increasing regulatory concerns regarding the disposal of lead-based ceramics, particularly when they are used in large-area applications with a high probability of human exposure.

The generated piezoelectric potential within a material is directly proportional to the applied strain and the magnitude of the piezoelectric coefficient. Nanostructures however are able to withstand larger deflections without failure and thus considerable piezoelectric power can be extracted even from materials with modest values of the piezoelectric coefficient d_{ijm}. Here we develop a novel approach for measuring the intrinsic piezoelectric response of the ZnO nanowire arrays. It is well known that the piezoelectric effect in crystalline materials with non-centrosymmetric structures, like ZnO, can be expressed as

$$d_{ijm} = \frac{\partial D_m}{\partial T_{ij}} \tag{1}$$

$$d_{ijm} = \frac{\partial S_{ij}}{\partial E_m} \tag{2}$$

where d_{ijm} is the piezoelectric coefficient, D_m the electric displacement vector, E_m the applied electric field, T_{ij} the applied stress, and S_{ij} the induced strain. $D_m = \varepsilon_0 E_m + P_m$, where ε_0 is the permittivity of free space and P_m is the induced electric polarization. Equations 1 and 2 are defined as the direct and converse piezoelectric effects, respectively.

However, for highly heterogeneous and anisotropic piezoelectric structures at the micro- or nano-scale, the tensor representation given in both eqs 1 and 2 may not be appropriate. For these piezoelectric structures, in practice, it is convenient to define an effective piezoelectric coefficient to describe their piezoelectric properties. Thus the above equations are modified as follows to address the piezoelectric response in ZnO nanowire arrays.

$$d_{eff} = \frac{\partial P}{\partial T} \tag{3}$$

$$d_{eff} = \frac{\partial S}{\partial E} \tag{4}$$

where d_{eff} is the effective piezoelectric coefficient and P, T, S, and E represent the induced polarization, the applied stress, the induced strain, and the applied electric field, respectively, all in scalar form. Unfortunately, even with these simplified mathematical expressions, piezoelectric measurements at the nanoscale still represent a formidable challenge, particularly for nanostructures affixed onto substrates. For instance, ZnO micro/nanostructures exhibit highly anisotropic elastic properties, which might substantially diverge from that of their bulk counterparts; it is consequently extremely difficult to precisely measure the induced deformation because of the size-dependent variability of elastic properties and the inevitable variations in geometry, morphology, and size under loading conditions.[21]

For ZnO micro/nanostructures, ultrasonic waves and atomic force microscopy (AFM) scanning have been used to measure the direct piezoelectric effect of ZnO NW arrays.[10,15] As

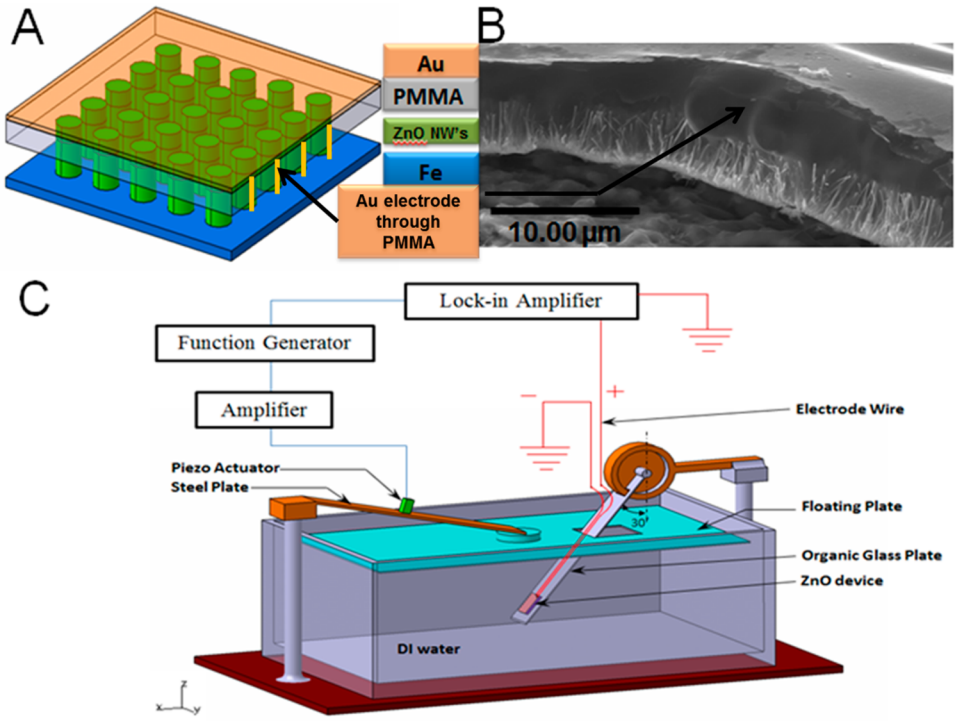

Figure 4. (A) Representative scheme and (B) cross-sectional SEM image of the functional ZnO nanowire array device. (C) Schematic illustration of the cantilever-beam apparatus designed for measuring the effective piezoelectric response of our ZnO nanostructures. Calibrated pressure wave propagation is used to apply a known stress and the induced flow of charge is detected using a lock-in amplifier.

another example of a measurement method, optical interferometry has been utilized to measure the converse piezoelectric effect of a microtubular ZnO structure.[22] Each method has its own advantages and drawbacks; for the ultrasonic wave and AFM scanning methods, measuring the induced current from the ZnO NW arrays is relatively straightforward but it is difficult to determine the corresponding piezoelectric coefficients because the applied stress values cannot be easily estimated.[10,15] The AFM scanning method is further plagued by the potential for interference from residual stray currents derived from electronic components at the AFM tip, which can interfere with the pA to nA piezoelectric currents generated upon deflection of individual nanowires. In contrast, optical methods allow precise determination of the piezoelectric coefficient but the technique is tedious and moreover sensitive to environmental factors, sample geometry, and artifacts.[22]

It should be pointed out that ZnO represents a distinct type of piezoelectric material, which is different from conventional ferroelectric materials. When undergoing deformation, charge separation induced within ZnO comprises contributions from both displacement of bound charges and the movement of free carriers; the latter arises from the semiconducting behavior of ZnO. Therefore, of particular relevance to observation of the direct piezoelectric effect within ZnO, the induced polarization is always accompanied by formation of a Schottky barrier at the contacts. To precisely evaluate the piezoelectric behavior of ZnO, the influence of the Schottky barrier needs to be addressed. However, most methods for measuring piezoelectricity of ZnO including the above mentioned ultrasonic wave perturbation and AFM scanning methods do not satisfactorily achieve this goal.

In this study, we have developed a new approach for reliable measurement of piezoelectricity in ZnO NW arrays, wherein not only can the applied stress be precisely determined but also the Schottky barrier problem can be directly addressed. Our measurement scheme is briefly summarized below.

As illustrated in panels A and B in Figure 4, the ZnO NW arrays are approximately regarded as a thin ZnO layer, whose direct piezoelectric response, i.e., the induced current, is measured as it undergoes continuous alternating bending-type deformation. This deformation is induced by a sinusoidal force at a drive frequency of 5 Hz applied via a commercially available piezoelectric actuator. Because the induced current is very small, the ZnO layer fabricated on a steel plate (which is mounted on an organic glass plate) is immersed in a tank filled with insulating silicone oil to prevent potential interference from stray currents. The silicone oil is considered to be an incompressible fluid. Consequently, as shown in Figure 4C, the applied sinusoidal force exerted on the floating plate can be effectively transferred from the surface of the silicone oil to the surface of the sample (the ZnO nanowires) on steel. Furthermore, this force can be precisely calibrated by using a load-cell setup. Thus, the applied force and stress values acting on the ZnO sample can be readily estimated in our measurement scheme.

As shown in Figure 4A, the steel plate beneath the ZnO nanowires is used as the ground electrode; a poly(methyl methacrylate) (PMMA) polymer layer is spin-coated onto the top surface of the ZnO layer, followed by deposition of a gold electrode layer atop the PMMA layer. The PMMA layer permits gold dendrites to reach the apices of the ZnO NWs at certain locations, as seen in the cross-sectional SEM image of Figure 4A. Here the PMMA layer is primarily used here to prevent short circuiting of the electrode and the steel plate. The induced current of the ZnO nanowire arrays can be measured by using the gold electrode. The applied sinusoidal force can be written as $F = F_0\cos(\omega t)$, where F_0 is a calibrated value, $\omega = 2\pi f$, and f = 5 Hz is the drive frequency. Next, the applied stress

acting on the ZnO layer can be estimated as $T = F_0 \cos(\omega t)/A$, where A represents the surface area of the ZnO layer. Within the linear range, the alternating charge separation, i.e., the induced current, across the ZnO layer as a manifestation of the direct piezoelectric effect can be measured and utilized to calculate the induced effective polarization as per

$$P_i = \frac{I_0 \cos(\omega t)}{\omega A} = \frac{I_0 \cos(\omega t)}{2\pi f A} \tag{5}$$

where I_0 is the induced current. Then the total polarization inside the ZnO layer will be

$$\sum P = P_i \pm P_S = \frac{I_0 \cos(\omega t)}{2\pi f A} \pm P_S \tag{6}$$

where P_S is the polarization generated by the Schottky barrier; the direction of P_S could be opposite to that of P_i, which is dependent upon how P_i is induced. Considering the range of the drive frequency (f = 5 Hz), we can approximately regard P_S as being constant at any given time. By using phase-sensitive detection based on a lock-in amplifier, components (dc values) of the detected current that are related to P_S are filtered out. Therefore, upon using phase-sensitive detection, the effective piezoelectric coefficient of the ZnO layer can be written as (note cancellation of the area term)

$$d_{\text{eff}} = \frac{P_i(t=0)}{T(t=0)} = \frac{I_0}{2\pi f F_0} \tag{7}$$

From the above explanation, it is clear that the influence of the Schottky barrier on piezoelectricity of the ZnO layer can be eliminated. Notably, the hydrostatic pressure in the oil tank also induces charge separation in the ZnO nanowires, but the induced charge values also do not vary with time and thus such a contribution to charge flow is also filtered out by the lock-in amplifier.

Here we must emphasize that eq 7 is derived under the assumption that the entire array of ZnO nanowires undergoes bending-type deformations. Clearly, given the layout of our sample and the measurement setup (Figure 4), this assumption might not be entirely correct. We can demonstrate this by considering a special case: if a hypothetical ZnO sample is vertically mounted inside the tank, i.e., wherein the angle between the ZnO plane and the vertical direction $\theta = 0°$ (θ is defined in Figure 4C). Clearly, under these conditions, only the nanowires near the top of the ZnO sample would be fully perturbed by the applied vertical pressure wave and would undergo bending-type deformations; in contrast, nanowires situated much below the surface, may not be perturbed at all. In this situation, d_{eff} measured via eq 7 would be much smaller than anticipated. Next we consider another special case wherein the sample is horizontally mounted, i.e., the angle between the ZnO layer plane and the vertical direction, $\theta = 90°$. Under this condition, based on theoretical considerations there ought not to be any bending-type deformations within the ZnO sample. Considering that the elastic modulus of ZnO can be as high as 200 GPa,[23] we can neglect the compressive deformation of the ZnO sample since the amplitude of the applied sinusoidal force is very small. Therefore, in this case, d_{eff} ought not to be measurable. Without loss of generality, we assume that the value of d_{eff} reaches a maximum at a particular angle, θ_p. When θ varies from 0 to θ_p, for convenience, we can modify eq 7 as follows.

$$d_{\text{eff}} = \frac{I_0 \sin\theta}{2\pi f F_0} \tag{8}$$

Using a series of calibrated F_0 values at different θ angles, we have measured the values of I_0 using the phase-sensitive detection scheme (Table 1). A linear correlation is observed between the applied stress and the induced polarization; the corresponding effective piezoelectric coefficients have been estimated by calculating the slopes of the plots shown in Figure 5. The measured piezoelectric coefficients are also summarized in Table 1. For our ZnO NW array sample, the optimal value of the effective piezoelectric coefficient, which is around 20 pC/N, has been obtained for $\theta_p \approx 33°$. These measured values agree with both recent theoretical calculations and the experimental data obtained for ZnO hexagonal microtubular structures (see ref 22 and the references cited therein). The experimental results also demonstrate that our measurement scheme can be used as a reliable and robust methodology to quantitatively evaluate the effective piezoelectric response of ZnO nanostructures. Notably, the piezoelectric response from tetrapods and nanocomb-like structures that do not show alignment along a specific crystallographic direction are at least an order of magnitude lower than measured for the oriented nanowires.

Table 1. Effective Piezoelectric Coefficients (d_{eff}) Measured for the Considered ZnO Nanowire Array

θ (deg)	d_{eff} (pC/N)
5	12.9 ± 0.3
10	12.6 ± 0.3
15	16.6 ± 0.3
20	18.2 ± 0.4
25	19.1 ± 0.4
30	19.9 ± 0.4

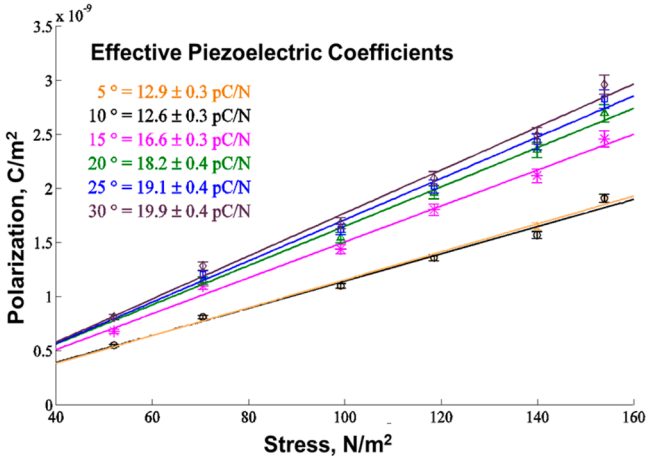

Figure 5. Polarization as a function of stress is plotted as a function of the angle. The calculated slopes, listed in Table 1, suggest significant anisotropic dependence of the effective piezoelectric response depending upon the specific angular deformation to which the ZnO nanowires are subjected.

CONCLUSIONS

In summary, we have developed a facile route to transform galvanized steel, a ubiquitous commodity material with widespread structural applications, to a functional piezoelectric

nanogenerator. Our approach is fully scalable to large areas and exceedingly robust to variations in synthetic parameters. The fabrication approach entails the oxidative processing of steel to obtain homogeneous vertically aligned ZnO nanowire arrays, which can be readily integrated within device architectures. In addition, we have developed a phase-sensitive detection scheme for precise piezoelectricity measurement of ZnO nanostructures. Our experimental studies have shown that the polarization induced within these structures due to piezoelectric response can be separated from that generated by the Schottky barrier based on our phase-sensitive detection scheme, which can further be generalized to explore the piezoelectric behavior of other semiconducting piezoelectric materials, such as AlN, GaN, and InN.

MATERIALS AND METHODS

ZnO nanowires were grown on double-sided galvanized steel obtained from Tata Steel. The galvanized steel has a thickness of 0.67 mm and nominal impurity content of 0.1% C, 1.5% Mn, 0.2% Si, 40 ppm N, 0.01% O, 0.002%S, 0.03% Ti and was plate galvanized with ∼15.0 μm of Zn metal on both sides using an in-house vaporization method developed by the Tata Steel. The substrate was placed on a ceramic boat at the center of a 1″ dia. quartz tube within a single zone furnace and the temperature was varied from 500 to 900°C with a controlled ramp rate of 10-30°C/min under Ar flow (1000-1600 sccm). Once the targeted temperature (∼600 °C) was reached, 2.5 sccm of O_2 was introduced for 30—60 s. Subsequently, the O_2 flow was switched off and the furnace was allowed to rapidly cool (∼20 °C/min) while maintaining Ar flow. Highly oriented nanowire arrays were obtained on the top (exposed) surface of steel, whereas nanocombs were observed on the bottom surface of the substrates. Morphological variations such as nanotetrapods and nanotubes were reproducibly realized by modification of process flow rates, heating rates, and pressure.

Phase identification was performed by XRD using a Rigaku Ultima IV diffractometer with Cu Kα radiation (λ = 1.5418 Å). Raman microprobe analysis was performed on a Jobin Yvon Horiba Labram HR instrument with excitation from a 514.5 nm Ar-ion laser. The dimensions, morphology, and elemental composition of the as-synthesized nanostructures were examined by SEM using a Hitachi SU-70 instrument operating at an accelerating voltage of 20 kV. A JEOL 2010 instrument operated at 200 kV was utilized to acquire bright- and dark-field TEM images.

Conformally adhered ZnO nanowire arrays on steel were spin-coated with a ∼10 μm layer of poly(methyl methacrylate) (PMMA) (Alfa Aesar) in *N*-dimethylformamide at 180 rpm for 30 s. Prior to spin-coating, the PMMA was filtered through a 0.4 μm filter assembly. The spin-coated sample was then placed in a preheated oven kept at 120°C for 25 min to evaporate the solvent and subsequently dried at room temperature for 24 h to form a thin transparent film on the surface of the sample. An electron-beam evaporator (BOC Edwards Auto 306) was utilized to deposit Au electrodes of ∼100.0 nm thickness on the bottom surface of the steel and on top of the PMMA layer. Using an oil-proof silver conductive epoxy (Ted Pella, INC CW 2400), two pieces of teflon-coated silver wire (Grass Technologies EW5AG) were attached to the deposited gold electrodes of the PMMA layer and the steel base of the sample, respectively. Subsequently, the sample was dried at room temperature for 24 h. Next, with the steel substrate functioning as the base electrode, the polymer/ZnO/steel assembly was mounted onto a glass substrate. A clamp with the organic glass plate was then affixed to a rotating optical post with marked angles, which allows the sample to be rotated at different angles with respect to the applied force on silicone oil. The experimental setup for pressure wave propagation (PWP) consisted of a small tank filled with silicone oil. During the measurement, a function generator (Stanford Research Systems model DS345) generated a sinusoidal signal at 5 Hz, which was transmitted to a modified piezoelectric actuator setup; the reference signal was further connected to a lock-in amplifier (Stanford Research Systems model SR830 DSP). The modified piezoelectric actuator setup comprises a voltage amplifier (Thorlabs model MDT694A), which sends its input signal (received from the function generator) to the piezoelectric actuator (Thorlabs model AE0505D18F). The actuator touches the mid-section of a steel plate as shown in Figure 5; the steel plate is positioned similar to a cantilever beam. For a known input of sinusoidal voltage, the force transferred from the midsection to the free end of the steel plate is calibrated separately using a load cell setup. The free end of the steel plate firmly touches the top surface of a floating plastic plate in its mid-section, and thus the silicone oil below the plate experiences a uniform force. The floating plate has a square-shaped open portion on one side, which acts as a passage for the organic glass plate to pass through and remains unattached to the inner sides of the tank. Equilibrium is maintained in the tank by allowing the excess silicone oil pressure to dissipate between the floating plate and the tank's inner wall. The sample end of the organic glass plate is immersed into a silicone oil tank through the opening in the floating flat plate. The top electrode wire from the sample is connected to the lock-in amplifier, thereby allowing detection of the induced current due to the bending of ZnO nanowires. The bottom electrode from the steel base is connected to the ground.

ASSOCIATED CONTENT

Supporting Information

Additional SEM images and schematic of ZnO unit cell (PDF). This material is available free of charge via the Internet at http://pubs.acs.org.

AUTHOR INFORMATION

Corresponding Author

*E-mail: sb244@buffalo.edu.

Notes

The authors declare no competing financial interest.

ACKNOWLEDGMENTS

This work was primarily funded by the Tata Steel Group. We also acknowledge partial support from the National Science Foundation under DMR 0847169. J.M.V. acknowledges partial support through a NASA Harriet G. Jenkins Fellowship. We appreciate helpful guidance from Dr. Debashish Bhattacharya.

REFERENCES

(1) Kelzenberg, M. D.; Boettcher, S. W.; Petykiewicz, J. A.; Turner-Evans, D. B.; Putnam, M. C.; Warren, E. L.; Spurgeon, J. M.; Briggs, R. M.; Lewis, N. S.; Atwater, H. A. *Nat. Mater.* **2010**, *9*, 239−244.
(2) Yanqing, W.; Yu-Ming, L.; Ageeth, A. B.; Keith, A. J.; Fengnian, X.; Damon, B. F.; Yu, Z.; Avouris, Ph. *Nature* **2011**, *472*, 74−78.
(3) Whittingham, M. S. *Dalton Trans.* **2008**, *40*, 5424−5431.
(4) Jen-Kan, Y.; Slobodan, M.; Douglas, T.; Joseph, V.; James, R. H. *Nat. Nanotechnol.* **2010**, *5*, 718−721.
(5) Wang, Z. L. *Adv. Funct. Mater.* **2008**, *18*, 3553−3567.
(6) Whittaker, L.; Patridge, C. J.; Banerjee, S. *J. Phys. Chem. Lett.* **2011**, *2*, 745−758.
(7) Wang, Z. L. *MRS Bull.* **2007**, *32*, 109−116.
(8) Wang, X.; Song, J.; Liu, J.; Wang, Z. L. *Science* **2007**, *316*, 102−105.
(9) Sheng, X.; Yong, Q.; Chen, X.; Yaguang, W.; Rusen, Y.; Zhong Lin, W. *Nat. Nanotechnol.* **2010**, *5*, 366−373.
(10) Muralt, P.; Polcawich, R. G.; Troiler-Mckinstry, S. *MRS Bull.* **2009**, *34*, 658−664.
(11) Marder, A. R. *Prog. Mater. Sci.* **2000**, *45*, 191−271.
(12) Wang, Z. L.; Song, J. *Science* **2006**, *312* (5771), 242−246.
(13) Qin, Y.; Wang, X.; Wang, Z. L. *Nature* **2008**, *45*, 809−813.
(14) Rout, T. K.; Gaikwad, A. V.; Lee, V.; Banerjee, S. *J. Mater. Res.* **2011**, *26*, 837−844.

(15) Velazquez, J. M.; Gaikwad, A. V.; Rout, T. K.; Rzayev, J.; Banerjee, S. *ACS Appl. Mater. Interfaces* **2011**, *3*, 1238−1244.
(16) Song, J.; Wang, X.; Riedo, E.; Wang, Z. L. *J. Phys. Chem. B* **2005**, *109*, 9869−9872.
(17) Cuscó, R.; Alarcón-Lladó, E.; Ibáñez, J.; Artús, L.; Jiménez, J.; Wang, B.; Callahan, M. J. *Phys. Rev. B* **2007**, *75*, 165−202.
(18) Jin, S.; Bierman, M. J.; Morin, S. A. *J. Phys. Chem. Lett.* **2010**, *1*, 1472−1480.
(19) Morin, S. A.; Bierman, M. J.; Tong, J.; Jin, S. *Science* **2010**, *328*, 476−480.
(20) Drum, M. *J. Appl. Phys.* **1965**, *36*, 824−829.
(21) Agrawal, R.; Espinosa, H. D. *Nano Lett.* **2011**, *11*, 786−790.
(22) Fu, J. Y.; Liu, P. Y.; Cheng, J.; Bhalla, A. S.; Guo, R. *Appl. Phys. Lett.* **2007**, *90*, 212907/1−212907/3.
(23) Azuhata, T.; et al. *J. Appl. Phys.* **2003**, *94*, 968−972.